Polymer 54 (2013) 2835–2849

Contents lists available at SciVerse ScienceDirect

Polymer

journal homepage: www.elsevier.com/locate/polymer

Feature article

Adsorption of proteins to functional polymeric nanoparticles

Nicole Welsch [a,b], Yan Lu [a,b], Joachim Dzubiella [a,b,c], Matthias Ballauff [a,b,c,*]

[a] Soft Matter and Functional Materials, Helmholtz-Zentrum Berlin für Materialien und Energie GmbH, Hahn-Meitner-Platz 1, 14109 Berlin, Germany
[b] Helmholtz Virtual Institute, Multifunctional Materials in Medicine, Berlin and Teltow, Germany
[c] Department of Physics, Humboldt University Berlin, Newtonstr. 15, 12489 Berlin, Germany

ARTICLE INFO

Article history:
Received 15 January 2013
Received in revised form
12 March 2013
Accepted 13 March 2013
Available online 23 March 2013

Keywords:
Protein adsorption
Colloids
Donnan-equilibrium

ABSTRACT

We review recent work on the adsorption of proteins on two types of well-defined colloidal particles, namely on i) spherical polyelectrolytes that consist of a solid core onto which long chains of a polyelectrolyte are attached, and ii) core–shell microgels that have a shell of crosslinked poly(N-isopropylacrylamide) (pNiPAm) chains. The latter system may bear charges as well by copolymerization with acrylic acid. The surface layers of both systems that have a thickness of ca. 50 nm create a microenvironment in which the salt concentration and the pH differ from the outside solution. Adsorption of various proteins to these particles is monitored by various methods including calorimetry, fluorescence spectroscopy and small-angle X-ray scattering. These investigations also include studies of the kinetics of adsorption. The secondary structure of the proteins can be analyzed in these systems by FT-IR spectroscopy. Their tertiary structure can be checked by measurements of the enzymatic activity. In some cases the adsorbed enzymes exhibit an even higher activity as compared to the free protein in solution. We review the application of these techniques to monitor adsorption of proteins to these particles. All data demonstrate that both types of particles present model systems that help us to explore the main driving forces of protein adsorption.

1. Introduction

The adsorption of proteins onto surfaces is a central problem in many areas of modern biotechnology and in the field of biomaterials [1,2]. Proteins will adsorb from aqueous solution to virtually any surface [3] and an understanding of the driving forces and the kinetics is of fundamental importance for many fields: On the one hand, adsorption of proteins must often be prevented in order to avoid adherence of bacteria or biofouling in medical applications [4]. On the other hand, immobilization of proteins is necessary in many technical applications in which enzymes are used as catalysts. Also, chromatographic purification of proteins requires a defined interaction of the biomolecules with the column material [5].

In recent years, adsorption of proteins to nanoparticles has become the subject of intense research [6]. The reason for this is given by the fact that nanoparticles will be immediately covered by a dense layer of protein when injected into the blood stream. This "corona" then will determine the response of the body to these particles [7–11] and a precise knowledge of the composition of the corona and its temporal evolution [12,13] is necessary for e.g. nanotoxicology, nanomedicine [14], and cell adhesion [15,16]. Moreover, adsorption may often be accompanied by a slow denaturation and the immune system of the body "sees" a denatured protein and not the material of which the nanoparticle is composed [17,18]. Moreover, protein adsorption is a kinetic phenomenon and the corona will change with time [12,13]. Highly mobile proteins adsorbed in an early stage will be replaced by other proteins with higher affinity in a complex series of adsorption and displacement steps [19–21].

The obvious importance of protein adsorption to nanotechnology has led to an enormous number of papers and reviews recently. Central to this question is the analysis of the possible driving forces and their modeling that should lead semi-quantitative predictions of the tendency of a protein to adsorb on a given surface [22–25]. The ultimate goal of such an effort must be the prediction of the composition of a corona of proteins as the function of the composition in solution.

Polymeric layers have often been used to minimize adsorption of proteins on surfaces. Coatings of linear [26] and of star-shaped polyethylene oxide [27] present the state-of-the-art approach to prevent protein adsorption on surfaces. On the other hand, it has shown that dense layers of charged polymers (polyelectrolyte

* Corresponding author. Department of Physics, Humboldt University Berlin, Newtonstr. 15, 12489 Berlin, Germany.
E-mail address: matthias.ballauff@helmholtz-berlin.de (M. Ballauff).

0032-3861 © 2013 Elsevier Ltd. Open access under CC BY-NC-ND license.
http://dx.doi.org/10.1016/j.polymer.2013.03.027

brushes; see Refs. [28,29]) lead to strong adherence of proteins to colloidal particles [30–32] and to planar surfaces [33–36]. Layers of crosslinked polymers attached to colloidal cores (core–shell microgels [37,38]) also attract proteins and may be used to immobilize enzymes [39–44]. In this way a polymeric layer attached to a surface opens the way to adjust the interaction of particles and macroscopic objects with proteins. The understanding of the various forces leading to attractive or repelling interaction of such a biointerphase is hence a central problem in nanotechnology.

Here we review recent investigations on the adsorption of proteins on colloidal particles having a well-defined polymeric shell. Fig. 1 shows both types of particles in a schematic fashion: The first type of particles bears long chains of a polyelectrolyte that are densely grafted to the surface of the core [28,29], the second system carries a dense network of poly(N-isopropylacrylamide) (pNiPAm) and poly(acrylic acid) (PAA) [37,38]. Both systems have a shell of a thickness between 30 and 150 nm. This shell can be synthesized in a very controlled fashion using various procedures developed in recent years [29,38]. Moreover, a wide variety of methods can be used to characterize these particles in solution with a precision down to the sub-nanometer range. These methods include scattering methods as small-angle X-ray and neutron scattering (SAXS, SANS) and cryogenic transmission electron microscopy (cryoTEM). If the concentrations are not too high, spectroscopic techniques working in the visible range as e.g. fluorescence spectroscopy can be applied. FT-IR spectroscopy which is not hampered by the turbidity of these aqueous suspensions can be used to determine the secondary structure of adsorbed proteins with great precision. Finally, most of these techniques can be applied in a time-resolved manner in order to assess the kinetics of protein adsorption.

The common feature of both systems is the charge affixed to the shells. Charges play a major role in protein adsorption since all proteins carry patches of positive and negative charges on their surface [45] that may interact with polyelectrolytes as e.g. DNA [46]. Hence, charge–charge interactions are important when considering the interactions of proteins with biointerphases [47].

This review is organized as follows: in Section 2 of this paper we shall discuss the general features of these particles. In particular, the role of charges will be considered. It can be shown that the surface layer of the particles displayed in Fig. 1 can be treated in terms of a Donnan-equilibrium. Section 3 will give a brief survey of the methods used so far to characterize both types of particles and their interaction with proteins. Section 4 then will be devoted to a discussion of the interaction of proteins with spherical polyelectrolytes and with core–shell microgels. A brief conclusion will wrap up the entire discussion. The survey will demonstrate that an in-depth understanding of protein adsorption to functional nanoparticles with advanced analytical techniques is possible. This opens the way for developing models with truly predictive power.

2. Polymeric colloids as model particles

2.1. Synthesis and characterization of the particles

The synthesis of spherical polyelectrolyte brushes [29] and of core–shell microgels [38] is well advanced and nearly monodisperse model systems can be prepared without problems. The characterization of the particles can be done as discussed recently for the case of core–shell microgels [37,38] and for spherical polyelectrolyte brushes [48]. Dynamic light scattering (DLS) has become one of the most important tool for the characterization of the overall size of both types of particles. This method is also uniquely suited to determine the colloidal stability of the particles in solution [49,50]. In case of the core–shell microgels it has been shown that the hydrodynamic radii determined by DLS agree well with the ones derived directly from cryogenic transmission electron microscopy (cryoTEM) [51,52]. Recently, cryoTEM has been combined with small-angle X-ray scattering (SAXS) in order to characterize core–shell microgels in detail [53]. The combination of both methods showed that the gel layer of these particles is rather compact. Moreover, the hydrodynamic radius provides a good measure for the overall size of the particles.

The SPB have also been under scrutiny by precise measurements of their zeta-potential in solution [54]. Moreover, their effective charge has been measured by dynamic light scattering and compared to current models [50]. Finally, recent investigations dealt with the dielectric spectroscopy of these particles in dilute aqueous solution [55]. These investigations together with earlier work summarized in Ref. [29] show clearly that in salt-free solution only small fraction of the counterions can evade the brush layer, most of the counterions are confined within the layer. The marked osmotic pressure within the brush ("osmotic brush" [28]) determines the properties of the particles in aqueous solution and their interaction with proteins. If the salt concentration is raised to sufficient ionic strength, this effect is strongly diminished and the systems behave nearly as uncharged systems ("salted brush"; Ref. [28]).

2.2. Charged polymeric interfaces: the Donnan-equilibrium

Fig. 2 displays the surface of the systems under consideration here in a schematic fashion: Charged polymers are densely grafted to a solid interface that may be either curved or planar. The

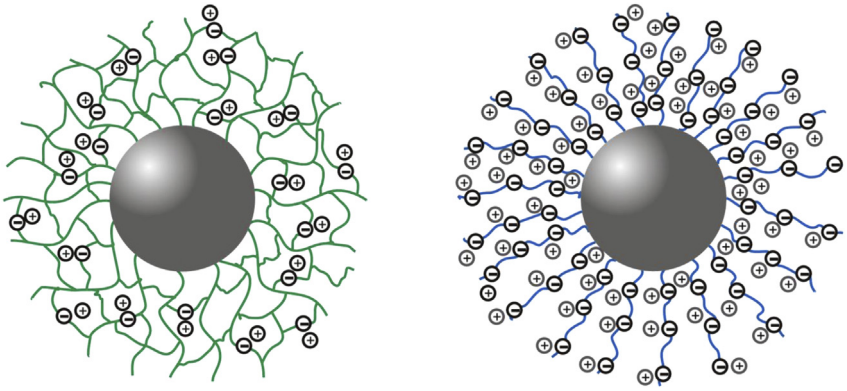

Fig. 1. Schematic presentation of the colloidal particles used in this study. Left-hand side: microgels consisting of a polystyrene core and a shell of crosslinked poly(N-isopropylacrylamide) (pNiPAm). Charges have been introduced by copolymerization with acrylic acid [37,38]. Right-hand side: spherical polyelectrolyte brushes consisting of a polystyrene core onto which linear chains of a polyelectrolyte are densely grafted [29].

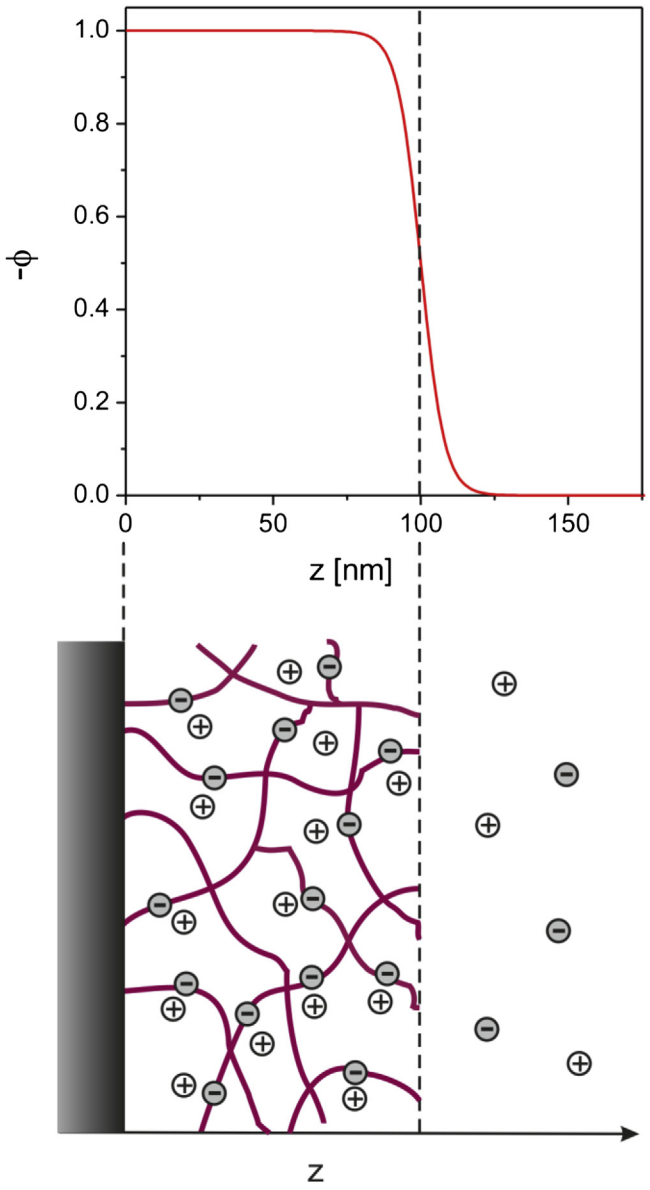

Fig. 2. The interface between a charged network and the bulk solution. Top: schematic presentation of the local electrostatic potential $\phi(z)$ (Donnan-potential) of a negatively charged brush with thickness of 100 nm as function of the distance z from the solid surface. Bottom: scheme of the surface onto which charged chains are appended the charge of which is balanced by a concomitant number of counterions. Most of these counterions are confined within the polymeric layer.

polymers may be linear as in the case of spherical polyelectrolyte brushes (SPB) or crosslinked as in case of the core–shell microgels. The charges affixed to the polymeric interlayer are balanced by counterions. In presence of added salt, co-ions will be present as well. It is now well-understood that the counterions balancing the charges of the polymer chains are mainly confined within the surface layer. For the case of polyelectrolyte brushes this has been shown a long time ago by Borisov et al. [56] and by Pincus [57] (see a general discussion of this point in Ref. [28]). In a similar manner it can be shown that charged nanoscopic network will retain most of their counterions [58]. As a consequence of this fact, the core–shell particles carry only a rather small net charge as determined by an electrophoretic experiment [54]. Thus, there will be an enormous osmotic pressure of these confined counterions which will determine the solution properties of the particles and their interaction with proteins.

In good approximation the confinement can be assumed as total and electrically neutral. Hence, the small fraction of counterions evading the charged layer (see Fig. 2) can be disregarded in first approximation. Therefore the concentration of the co- and counterions can be treated in terms of a Donnan-equilibrium. The equilibrium between the ions inside and outside then will lead to a concentration of counterions within the network/brush given by (see e.g. Ref. [28])

$$\frac{c_{s,particle}}{c_{salt}} = \left(\frac{\alpha c_g}{2c_{salt}}\right) + \sqrt{\left(\frac{-\alpha c_g}{2c_{salt}}\right)^2 + 1} \tag{1}$$

while the concomitant Donnan-potential reads

$$\Delta\phi = e^{-1} k_B T \ln\left[\left(\frac{-\alpha c_g}{2c_{salt}}\right) + \sqrt{\left(\frac{-\alpha c_g}{2c_{salt}}\right)^2 + 1}\right] \tag{2}$$

where $c_{s,particle}$ is the salt concentration within the brush or microgel layer, c_{salt} is the salt concentration in the bulk solution, α is the fraction of negatively charged monomer units within the network/brush, and c_g is the concentration of acidic monomer units in the network/brush. When protons are used as counterions, the pH in the network will be much lower than in the solution and a partial protonation of proteins inside will result. Close to the isoelectric point of a given protein, this effect may even lead to charge reversal [59,60]. In this case a strong interaction of the surface layer with the protein must result and marked adsorption will occur. Evidently, charge–charge interaction matter in this case and protein adsorption must depend strongly on the overall salt concentration c_{salt}. This is found indeed for planar [33–36] and spherical polyelectrolyte brushes [30–32].

The foregoing considerations have assumed full localization of the counterions in the surface layer. However, this assumption presents an idealization because there will be a transition zone with a finite concentration of counterions. This surface layer is shown schematically in Fig. 2. The surface layer will hence assume a net charge that can be detected by electrokinetic experiments [50,54]. This net charge will repel proteins having the same charge or attract proteins with opposite charge. Moreover, the Donnan-potential eq. (2) will vary in a continuous fashion when going from the bulk solution where $\Delta\phi = 0$ to the bulk of the layer where $\Delta\phi$ assume a constant value. As a consequence of this, the local electric field following as the negative spatial derivative of $\Delta\phi$ will be non-zero in this transitory layer. Since the uneven distribution of charges on the surface of proteins lead to a dipole moment of appreciable magnitude, this non-zero electric field may then lead to a further attractive force between the surface layer and the protein. A quantitative estimate of the magnitude of this effect, however, is not available at present.

3. Protein adsorption

3.1. Techniques

3.1.1. Isothermal titration calorimetry (ITC)

Since the radius of the particles is in the colloidal domain, that is, around 100 nm, suspensions of such particles create an enormous surface in solution. Protein adsorption therefore will lead to strong enthalpic effects that can be precisely monitored by isothermal titration calorimetry (ITC). Hence, ITC has become one of the foremost tools for the study of the interaction of nanoparticles with proteins [31,32,39,42,61–71]. Extended discussions of the application of ITC to the particles under consideration here were presented recently [32,44].

Fig. 3 displays typical ITC results of an adsorption reaction on colloidal particles. The general measuring principle of ITC is as follows: ITC measures the time-dependent evolution of heat Q upon injections of an aliquot of protein into a solution of microgel against a reference cell filled with water. After completion of the experiment the raw ITC data can be integrated over time to give the incremental heat ΔQ as function of the molar ratio between the protein and microgel. In a separate experiment the heat of dilution of the protein is measured and subtracted. After correction for the heat of dilution of the protein the total heat change after each injection can be fitted with an appropriate equilibrium binding model to determine the enthalpy ΔH_{itc}, the binding constant K, and the number of binding sites N [32,44].

A point that requires special attention is the attainment of equilibrium. The method applied usually for the evaluation of the ITC data assumes a Langmuir isotherm, that is, equilibrium between the adsorbed and the non-adsorbing proteins in solution (see below). For the particles shown in Fig. 1 it could be shown that equilibrium is reached indeed. This point will be discussed in further detail when discussing the kinetics of protein adsorption to microgels. For hard surfaces, however, protein adsorption is often irreversible. Hence, titration curves describing the growth of the adsorbed layer as the function of added protein must be interpreted with caution [24].

If equilibrium can be firmly established, experiments done at different temperatures offer the unique possibility to explore the entire thermodynamics of protein adsorption. In principle, the dependence of K on temperature should be related directly to ΔH_{itc}, that is, ΔH_{itc} should coincide with the enthalpy ΔH_{vH} derived from application of van't Hoff's equation to $K_b(T)$:

$$\left(\frac{\mathrm{d}\ln K}{\mathrm{d}T^{-1}}\right)_p = -\frac{\Delta H_{bind}}{R} \tag{3}$$

ΔS_{bind} can also be extracted from the temperature dependence of the free energy as follows:

$$\frac{\mathrm{d}\Delta G_{bind}}{\mathrm{d}T} = -\Delta S_{bind} \tag{4}$$

However, recent investigations by ITC on related problems such as protein–protein interaction or protein unfolding have revealed serious discrepancies between the two enthalpies [72,73]. This finding has led to a number of investigations [74,75] and a critical review thereof may be found in Ref. [73]. For the case of the adsorption of proteins to SPB this question was recently addressed by Ref. [32], and the case of protein binding to core–shell microgels was discussed in Ref. [42]. Both investigations led to the conclusion that the total enthalpy ΔH_{itc} must be split up into at least two parts:

$$\Delta H_{itc} = \Delta H_{bind} + \Delta H_{res} \tag{5}$$

where only ΔH_{bind} is related to the process of the binding of the protein to the particles. The second part ΔH_{res} is due to unrelated equilibria, that is, to processes that proceed independently of the process of binding. In case of the core–shell microgels ΔH_{res} was shown to be partially caused by the protonation of lysozyme within the gel layer [42]. For the case of the adsorption of RNase A to cationic SPB, ΔH_{bind} was even found to be zero and the binding of the protein was entirely driven by entropy. Thus, ΔH_{res} acted as a "marker enthalpy" in the latter case allowing us to measure a binding process which is not leading to any enthalpic effect.

ITC measurements can also be used for determination of catalytic activity of bound enzymes [76]. Here the enthalpy of the enzymatic reaction is utilized and enzyme activities can be measured with excellent accuracy. This method is strongly recommended in cases where a convenient colorimetric assay is missing.

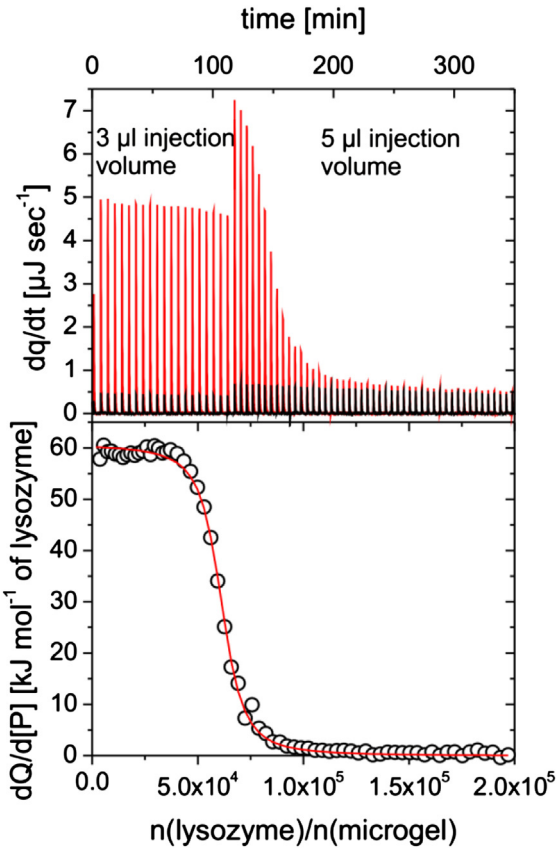

Fig. 3. Top: raw ITC data of binding of lysozyme to microgel particles at 298 K in 10 mM MOPS buffer pH 7.2. The black spikes are the heat of dilution of the protein and the colored spikes are the change of heat corresponding to each injection of protein into the microgel dispersion. Bottom: the lower panel shows the integrated heats Q of each injection of lysozyme (circles) after subtraction of the dilution signal from the overall signal. The solid line represents the fit based on the Langmuir isotherm (see below). Taken from Ref. [42].

3.1.2. *Small-angle X-ray scattering (SAXS)*

Small-angle X-ray scattering (SAXS) and small-angle neutron scattering (SANS) are the methods of choice when the radial density profile of spherical particles are to be determined in solution [77]. In general, SAXS is sensitive to the difference between the electron density of the dissolved object and the dispersing medium which is water in all cases discussed here. Thus, the measured scattering intensity $I(q)$ (q: magnitude of scattering vector; $q = (4\pi/\lambda)\sin(\theta/2)$, λ: wavelength of radiation, θ: scattering angle) follows as

$$I(q) = B^2(q) \tag{6}$$

where the scattering amplitude is given by

$$B(q) = 4\pi \int_0^\infty [\rho(r) - \rho_m] \frac{\sin qr}{qr} r^2 \,\mathrm{d}r \tag{7}$$

Here $\rho(r)$ denotes the radial electron density whereas ρ_m is the respective quantity of the dispersing medium. The core–shell particles shown in Fig. 1 have been extensively investigated using SAXS and Fig. 4 displays a typical example of an analysis of an SPB by this method [78]. Here $I(q)$ is shown together with a fit deriving from the radial excess electron density $\Delta\rho = \rho(r) - \rho_m$. This profile

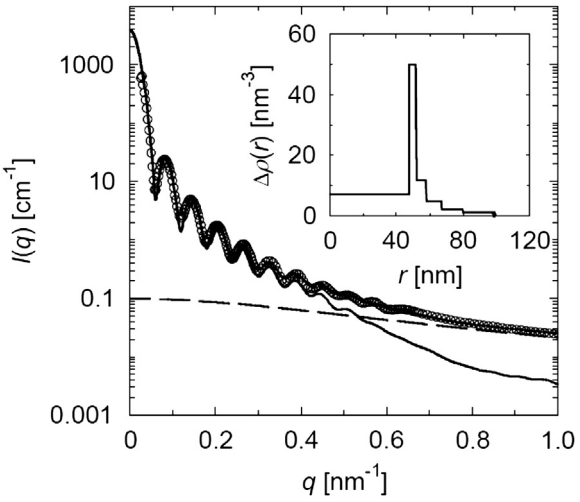

Fig. 4. SAXS-intensity of a spherical polyelectrolyte brush (weight fraction: 0.045). The circles give the measured intensity and the solid line shows the optimal fit (see text). The dashed line refers to the contribution to $I(q)$ deriving from the fluctuations of the brush layer affixed to the surface of the particles. The inset presents the excess electron density $\rho(r) - \rho_m$ as the function of the radial distance r which has been obtained from this fit. Taken from Ref. [78].

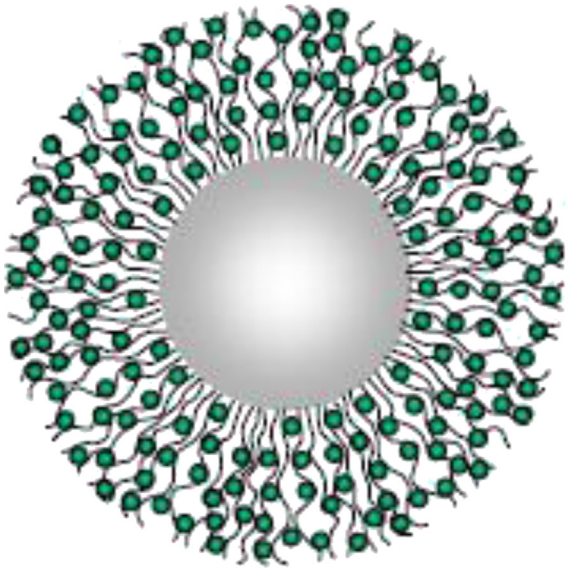

Fig. 5. Scheme of a composite of a spherical polyelectrolyte and a protein (BSA) as measured by SAXS. The scheme is drawn to-scale. Taken from Ref. [78].

has been approximated by 5 discrete layers because of the finite resolution of the method. There is an additional contribution at higher scattering angles which is due to the fluctuations of the chains attached to the core. Interaction between different particles leads to depression in the region of smallest q. For most applications of this method to the particles under consideration here, this effect may be safely dismissed (see Ref. [78] for a detailed discussion of this point).

SAXS has been extensively used for the analysis of protein uptake by spherical polyelectrolyte brushes [78–81]. Proteins have a strong X-ray contrast in water [78] and their uptake by the SPB leads to a marked change of the scattering curves. Evaluation of these data leads to the radial distribution of the adsorbed proteins within the layer and to the total amount of adsorbed protein τ_{ads}. This can be seen directly from eq. (6): For $q = 0$, that is, for vanishing scattering angle the scattering amplitude is the integral over the entire excess electron density of the particles. The comparison of this quantity for particles with and without protein then leads directly to the amount of adsorbed protein inasmuch as the excess electron density of a single protein is known with precision. The data thus obtained can then be compared to results obtained by other methods [78,79,81]. Given the various sources of error, the agreement is reasonably good.

The most significant result obtained by SAXS is the radial structure of the particles in solution. Fig. 5 displays a to-scale scheme of an SPB with adsorbed BSA molecules derived from SAXS [78]. The large number of adsorbed protein molecules is directly visible. Moreover, the analysis of the SAXS-data demonstrated that the BSA is strongly correlated to the polyelectrolyte chains. This is another clear indication for the importance of electrostatic interaction for protein adsorption.

3.1.3. Fluorescence spectroscopy

Fluorescence spectroscopy has been repeatedly used [43,82–84] to study protein adsorption on spherical polyelectrolyte brushes. In most cases, this technique requires fluorescent-labeled proteins. The labeling procedure, however, has to be well designed in order to prevent changes of the native conformation of the labeled protein. Moreover, one should always be aware that the introduction of fluorescent tags may modify the interactions with nanoparticles by changing the net charge of the protein or by directly interacting with the particle surface. Nienhaus and coworkers used a green fluorescent protein (mEosFP) in the fluorescence experiments superseding fluorescence labeling [82]. In this study they monitored the uptake of mEosFP by individual SPB particles using confocal laser scanning fluorescence microscopy with single molecule sensitivity (CLSM) [82]. They could demonstrate that the protein is taken up by the polyelectrolyte layer on the surface if the salt concentration is low in the system. Raising the salt concentration then led to a nearly complete release of the protein. Moreover, the well-known photo-physics of this protein can be utilized to analyze the tertiary structure of the adsorbed protein and the released protein as well. Here the authors found that virtually no change or partial denaturation had happened [82].

The intrinsic protein fluorescence from tryptophan residues has also been used to analyze changes of the microenvironment upon binding to nanoparticles and of the protein tertiary structure [85]. However, it has to be noted that fluorescence of many particles, such as systems based on polystyrene, strongly interferes with the fluorescence signal of the aromatic protein residues in the ultraviolet range. In this case, the analysis requires the presence of additional fluorescent groups emitting in, e.g. the visible range.

Fluorescence spectroscopy with labeled proteins was recently used by us to monitor the uptake of lysozyme by a core–shell microgel [42]. Because of the lower pH value inside the charged network the intense fluorescence of the fluorescein-labeled protein is quenched. Thus, the time-resolved analysis of the binding of proteins to colloidal particles as well as to the study of competitive protein adsorption can be done by monitoring the time-dependent decay of the fluorescence (see Section 4).

In a series of elegant experiments Nienhaus and coworkers employed fluorescence correlation spectroscopy (FCS) to monitor protein adsorption on small (10–20 nm in diameter) and fluorescent inorganic nanoparticles [86], a review has been given recently [24]. They found that proteins bind with micromolar affinity to the particles to form a protein corona of thickness of ~3.3 nm [86]. The group also performed time-resolved fluorescence quenching studies with labeled protein to monitor the association of protein molecules with the hard nanoparticles.

Rotello and coworkers analyzed the exchange of a green fluorescent protein (GFP) by other proteins from the surface of gold nanoparticles exploiting the fluorescence quenching capabilities of this metal [87,88]. They elegantly showed that the GFP/gold nanoparticle complexes provide an effective system suitable for sensing of proteins in human serum containing a high overall protein amount of ~70 g L^{-1}. Thus, it appears clear that techniques based on fluorescence spectroscopy offer a variety of possibilities to obtain quantitative data on the interactions between proteins and nanoparticles which would be useful for a multitude of nanoscience applications.

3.1.4. Fourier-transform infrared (FT-IR) spectroscopy

Fourier-transform infrared (FT-IR) spectroscopy is a valuable technique to study the secondary structure of proteins in aqueous solution [89,90] as well as in the adsorbed state [79,91–97]. Unlike other techniques, e.g. circular dichroism, it is not limited to transparent solutions and can be applied to samples which strongly scatter light such as latex particles. The protein secondary structures are analyzed on the basis of the absorption pattern of the amide bonds. The characteristic bands are the amide I and II vibrational modes of the protein amide groups which appear in the IR regime between 1500 and 1700 cm^{-1}. These are the most sensitive vibrational modes to quantify the secondary structure elements, i.e. the α-helix and β-sheet content. Fig. 6 displays the difference FT-IR spectra obtained from BSA absorbed to a spherical polyelectrolyte brush [91]. The amide I and II band can be determined precisely despite the fact that the composite particles are dispersed in water. In case of the SPB particles used in the study [91] the absorption of the particles in the wavelength region where the protein amide vibrational modes appear is nominal and makes data evaluation simple. On the other hand, it has been shown that the adsorption of proteins to particles containing amide bonds in their chemical structure can be treated by FT-IR spectroscopy as well [41,42]. Therefore, the spectral contributions of the carrier particles must be carefully analyzed and separated from the intensities of the protein amide modes. Hydrogels and microgels based on pNiPAm, for example, show such amide I and II modes [98–100]. It has to be noted that the hydration of the amide groups of uncharged gels is very sensitive toward changes of the temperature rendering the IR spectra of the gels temperature-dependent, too [98,100].

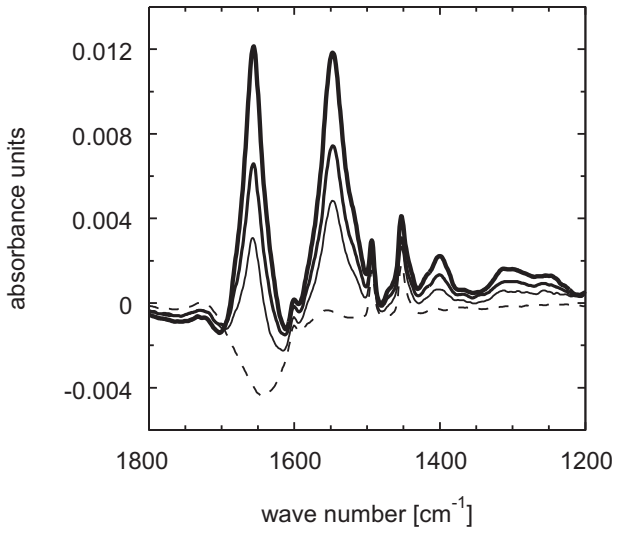

Fig. 6. FT-IR spectra of a spherical polyelectrolyte brush loaded with bovine serum albumin of varying concentration. Amounts of adsorbed protein: 1116 (bold line), 828 (semi-bold) and 577 (thin line) mg BSA per g of carrier particle. The spectra of the pure SPB particle are plotted for comparison (dashed line). The dominant signals are assigned to the amide I and II bands of the protein. All spectra are scaled to a concentration of 1 wt% of the carrier particle. Taken from Ref. [91].

The shape and intensity of the protein amide bands gives information about the secondary structure of proteins [101–103]. One approach is based on shape recognition of the IR bands and a calibration matrix created from IR spectra of proteins with known structure. Usually, these structures were determined by performing X-ray crystallography. This calibration set is then analyzed by using a partial least square (PLS) method and the secondary structure of the unknown protein is calculated [102,103]. The standard deviation of the secondary structural elements with this method was determined to 4.8% for the α-helix, 3.7% for the β-sheet and 5.1% for random coil segments [102]. Several studies demonstrate that this analysis is successfully applied to proteins immobilized on spherical polyelectrolyte brushes [79,91,92,104] as well as on core–shell microgels [41,42].

3.2. Protein adsorption: equilibrium isotherm

Binding of proteins from single protein solutions on the core–shell microgels is well-described by the Langmuir adsorption isotherm [41,42,44]. The Langmuir isotherm is an equilibrium binding model and, thus, requires a dynamic equilibrium between adsorbed molecules and those in the surrounding solution. It has been applied to protein adsorption on a variety of systems, including solid surfaces [105], silica nanoparticles [105,106], polymer brushes [31,107,108] as well as microgels [39,41–43,62,109]. An in-depth discussion of the Langmuir isotherm and its application to protein adsorption has been given recently [44]. In principle, the Langmuir isotherm describes the adsorption/desorption equilibrium between a solute and a solid system having N binding sites. Note that this model is not restricted to the description of monolayers. The only prerequisite for the application of this model is equilibrium, that is, the measured isotherm must result from an adsorption/desorption equilibrium. This condition is often not fulfilled and must be checked in each case (see above).

The Langmuir isotherm relates the fraction of adsorption sites in the gel containing bound protein Θ to the binding constant K given by Ref. [110]

$$\Theta = \frac{K[P]}{1 + K[P]} \tag{8}$$

where $[P]$ is the concentration of protein in solution. For a microgel containing N adsorption sites, Θ is N_b/N, with N_b as the number of proteins bound per particle. It must be noted that this isotherm requires that N is a constant independent of any interaction between the adsorbing molecules. This excludes the formation of additional layers due to strong interactions between the adsorbed proteins.

Recently, a new derivation of the Langmuir isotherm could be presented which is based on an excluded volume model [44]: The gel is modeled as a given volume in which the proteins can move freely, no immobilization on a fixed site is assumed. Confinement of space then leads to packing constraints that counteract the electrostatic attraction modeled in terms of a Donnan-potential. It is important to note that the conventional Langmuir isotherm can be recovered from this model as the limiting for low packing fractions of the protein, that is, for packing fractions for which the excluded volume constraint can still be approximated by a second virial coefficient. Hence, the Langmuir isotherm is a far more general approach than anticipated from its classical derivation [44].

In principle, the Langmuir isotherm can be generalized to the competitive adsorption [111] of two or more proteins to a given particle. Here it is requires that N is of the same magnitude for both competing proteins, that is, there is the same number of places onto which both proteins may adsorb. This implies that both adsorbing molecules are of the same size and have a similar interaction with the adsorbent. Recently, we applied this model to the competitive adsorption of lysozyme (A) and cytochrome c (B) (see Ref. [43] for an extended discussion):

$$\Theta_A([P]_A,[P]_B) = \frac{K_A[P]_A}{1+K_A[P]_A+K_B[P]_B} \quad (9)$$

$$\Theta_B([P]_A,[P]_B) = \frac{K_B[P]_B}{1+K_B[P]_B+K_A[P]_A} \quad (10)$$

where $[P]_A$ and $[P]_B$ are the concentration of unbound protein A and of the unbound competing protein B in solution, respectively. K_A and K_B are the respective binding constants obtained from e.g. ITC experiments for the adsorption of the respective single protein. It has to be noted that the competitive Langmuir isotherm is solely based on the binding constants of the individual proteins and does not include cooperative phenomena. Thus, it is assumed that proteins of type A do not influence the binding affinity of the proteins of type B and vice versa. Hence, application of eqs. (9) and (10) to experimental data measured on binary mixtures of proteins can decide whether the adsorbed proteins strongly interact within the particles or whether they just compete for the N total binding sites available on the particle. A first successful demonstration of the validity of this approach has been given recently [43]. Given the fact that virtually all practical applications involve mixtures of many proteins, modeling of the competitive adsorption is perhaps the most important task in the immediate future.

In the case of spherical polyelectrolyte brushes the adsorption isotherm required at least the combination of two Langmuir steps. In order to model the very strong adsorption of e.g. of BSA onto SPB, an expression based on the usual BET-isotherm has been developed [30,112]. The resulting expression reads [112]

$$\frac{\tau_{ads}}{\tau_{ads,M}} = \frac{z w_{ads}[P]^{1/n}}{\left(1-w_{ads}[P]^{1/n}\right)+\left[1+(z-1)w_{ads}[P]^{1/n}\right]} \quad (11)$$

where $\tau_{ads,M}$ denotes the maximum mass of protein needed for the strongest adsorbed layer and $zw_{ads}[P]$ with $z>1$ is the probability of the adsorption of a protein molecule onto this layer. The probability for the adsorption of subsequent layers is only $w_{ads}[P]$. Hence, τ_{ads} as function of $[P]$ may be described in terms of four adjustable parameters $\tau_{ads,M}$, w_{ads}, z and n. It should be noted that eq. (11) describes the case in which the adsorbed proteins interact heavily with each other. Hence, the analysis in terms of a conventional Langmuir isotherm would no more be applicable.

3.3. Protein adsorption: kinetics

Colloidal particles provide a large surface in a small confinement. Hence, adsorption of proteins will lead to a marked change of the system that can be detected by a wide variety of methods as a function of time, most notably by time-resolved fluorescence spectroscopy [43] and by time-resolved SAXS [80]. As discussed in the preceding section, protein adsorption on both types of particles shown in Fig. 1 can be modeled by a single or a two-step Langmuir isotherm. As demonstrated for the first time recently [43] (see Fig. 7), the kinetics of protein adsorption can be modeled in terms of the kinetic Langmuir model [113]:

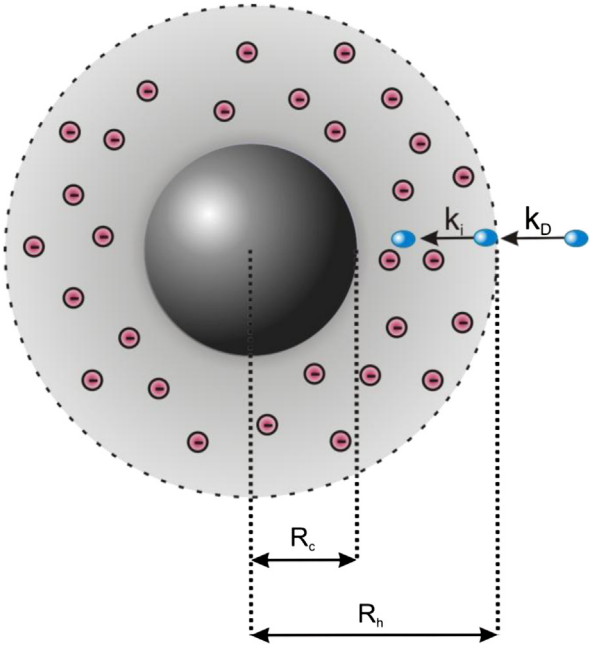

Fig. 7. Schematic representation of the uptake of proteins by the negatively charged microgel network with a core of radius R_c and an overall hydrodynamic radius R_h (counterions not shown). Protein diffusion on the surface of the microgel is described by the rate constant k_D while the motion of the protein along the polymer chains of the gel network is determined by the rate constant k_i. Taken from Ref. [43].

$$\frac{d\Theta}{dt} = k_{on}\frac{[B][P]}{N[M]_t} - k_{off}\frac{[PB]}{N[M]_t} = k_{on}(1-\Theta)([P]_t - N\Theta[M]_t) - k_{off}\Theta \quad (12)$$

where k_{on} and k_{off} is the adsorption and desorption rate, respectively, $[M]_t$ is the total microgel concentration and $[P]_t$ is the total protein concentration in solution. The analytical solution for $\Theta(t)$ was derived by Azizian [113] and can be used directly to fit the data deriving from time-resolved experiments. Eq. (12) can be further simplified by using the relationship $K = k_{on}/k_{off}$ and by making the substitution k_{off} for k_{on}/K. The adsorption constant K can be determined e.g. from the ITC analysis of the equilibrium state and the only unknown in eq. (12) is the rate constant of adsorption k_{on}.

For diffusion controlled binding reactions the diffusion flux of protein molecules to the adsorption sites becomes the rate-determining step. As visualized in Fig. 7, the motion of the proteins to the adsorption sites need to be divided into two contributions which are quantified by the rate constants k_D and k_i: First, the protein diffuses from the bulk solution to the microgel surface which is characterized by the rate constant k_D. This parameter can be described by the rate constant of diffusion-limited association reactions between small and large molecules with perfectly absorbing boundary conditions (Smoluchowski rate) [114]:

$$k_D = 4\pi D_0 R \quad (13)$$

where D_0 is the diffusion coefficient of the protein in solution, R is the radius of the microgel. Thus, k_D follows from the diffusion coefficient of the protein under consideration which is typically about 10^{-10} m^2 s^{-1} and from the hydrodynamic radius of the microgel R_h which is used for R. The second contribution to k_{on} considers the uptake of the proteins into the three-dimensional charged microgel network. This term will be described by the parameter k_i. Consequently, k_{on} is expressed by k_D and k_i, with k_i being the sole unknown parameter of eq. (12):

$$k_{on}^{-1} = \left(\frac{k_D}{N}\right)^{-1} + \left(\frac{k_i}{N}\right)^{-1} \quad (14)$$

The above model has first been applied to the adsorption of lysozyme to a core–shell microgel [43]. In this case, the two time constants k_D and k_i were determined to be of comparable size.

4. Survey of results

Table 1 gives a survey of all references related to studies on proteins adsorption on the systems shown in Fig. 1. In the following a brief survey on the main results obtained so far on both systems will be given.

4.1. Strength of interaction and driving forces

All investigations done so far on the systems shown in Fig. 1 lead to the conclusion that there are two main driving forces, namely hydrophobic attraction and electrostatic interaction. The latter force is weakened by raising the ionic strength while hydrophobic attraction is nearly independent of small salt concentrations. Hence, the influence of both forces can be analyzed by measuring the dependence of the adsorbed amount of protein at different salt concentrations [30,31]. This can be done also by ITC measurements run at different salt concentrations [31,32,42–44]. Moreover, the release of bound protein upon raising the ionic strength is a clear indication for the important role of electrostatic forces. This effect has been demonstrated for the spherical polyelectrolyte brushes by fluorescence spectroscopy [82] and by direct determination of the amount of released protein after stepwise addition of salt [117].

A quantitative analysis of the influence of electrostatic interaction of proteins with charged polymeric layers must in principle consider two different cases: i) A *weakly charged* layer in which the distance of the charges on the polymer chains is larger than the Bjerrum-length l_B giving the distance at which the electrostatic interaction between two probe charges is exactly k_BT; ii) a *strongly charged* system in which the distance of the charges on the polymer chains is much smaller. Case i) refers to the weakly charged ***microgels*** considered recently [42–44] while all ***spherical polyelectrolyte brushes*** studied so far by us refer to case ii).

A quantitative analysis has recently been done for case i) and applied to ***weakly charged microgels*** [44]. The protein is modeled as a sphere with a given radius R_p and characterized by a net surface charge number z_p. The surface layer of the microgel is characterized by the Donnan-potential $\Delta\tilde{\phi} = e\beta\Delta\phi$ as lined out in Section 2.2. However, during the process of protein binding to the charged network the Donnan-equilibrium will be modified by the net charge and amount of entering proteins. This leads to the change of electrostatic interactions with progressing protein sorption and, thus, to cooperative binding phenomena. Consequently, the total binding constant K becomes a function of the protein concentration and needs to be split up into an intrinsic part K_0 and an electrostatic part via

$$K(x) = K_0 \exp[-\beta\Delta G_{el}(x)] = \frac{\Theta(x)}{[1-\Theta(x)][P]} \quad (15)$$

where $x = [P]_{tot}/[M]_{tot}$ is the molar ratio between protein and microgel with $[P]_{tot}$ and $[M]_{tot}$ as the total protein and microgel concentration in the volume, respectively. Thus, the Gibbs binding free energy is the sum of the intrinsic and x-independent binding free energy $\Delta G_0(x)$ and the electrostatic contribution $\Delta G_{el}(x)$, that is $\Delta G(x) = \Delta G_0(x) + \Delta G_{el}(x)$. The intrinsic part $\Delta G_0(x)$ is defined by the binding constant K_0 which reads

$$\beta\Delta G_0 = -\ln(K_0/v_0) \quad (16)$$

where v_0 is the "standard volume" which describes the "effective" configurational volume in one binding box.

As shown in our recent paper [44], the term $\Delta G_{el}(x)$ contains two terms:

$$\beta\Delta G_{el} = z_p\Delta\tilde{\phi} - \frac{z_p^2 l_B}{2R_p}\left(\frac{\kappa_g R_p}{1+\kappa_g R_p} - \frac{\kappa_b R_p}{1+\kappa_b R_p}\right) \quad (17)$$

The first term describes the overall electrostatic interaction of the charged sphere with the Donnan-potential. The latter, however, must be corrected for the change of the total net charge by the charge of bound protein as outlined in Refs. [43,44]. The second term is related to the Born-energy of the charged protein sphere in an environment characterized by the inverse screening length $\kappa_g = \sqrt{8\pi l_B c_g}$ with c_g as the mean charge density in the gel network. Here the subscript g refers to the gel phase while b refers to the bulk phase. Since κ_g is larger in the gel phase, the overall contribution to ΔG_{el} is negative, that is, favorable. An extended discussion of this term including its derivation is given in Ref. [44]. Here it suffices to state that this term that is of non-negligible magnitude when compared to the first term in eq. (17) is related to a better screening of the surface charges of the protein in an environment with higher salinity, *i.e.*, in the gel as opposed to the bulk phase. If the salt concentration in the bulk is raised, both terms in eq. (17) diminish and the electrostatic driving force for the uptake of protein vanishes.

Using this model the free energy induced by the uptake of protein could be analyzed in detail. The magnitude of the hydrophobic attraction of lysozyme to a pNiPAm-network was found here to be of the order of $-7k_BT$ per protein molecules which corresponds to 2–3 hydrophobic contacts of one protein with pNiPAm

Table 1
Survey of investigations done on the adsorption of proteins to spherical polyelectrolyte brushes (SPB) and core–shell microgels.

	SPB anionic PAA[a]	SPB, anionic PSS[b]	SPB cationic[c]	Microgel uncharged[d]	Microgel charged[e]
BSA	[30,78,80,83,84,91,117]	[78,79,91]			
β-Glucosidase	[112]	[112]		[41]	[43]
β-Lactoglobulin	[91]	[81]			
Ribonuclease A	[78,91]	[31,78]	[32]		
Glucoamylase	[112,123]	[112]			
Bovine hemoglobin		[79]			
mEosFP	[82]				
Lysozyme					[42–44]
Cytochrome c					[43]

[a] Poly(acrylic acid).
[b] Poly(styrene sulfonic acid).
[c] Poly([2-(methacryloyloxy) ethyl] trimethylammonium) (PMETA).
[d] Core: polystyrene, shell: poly(N-isopropylacrylamide) crosslinked by 2.5% N, N′-methylenebisacrylamide.
[e] Core: polystyrene, shell: poly(N-isopropylacrylamide) + 10% poly(acrylic acid) crosslinked by 5% N, N′-methylenebisacrylamide.

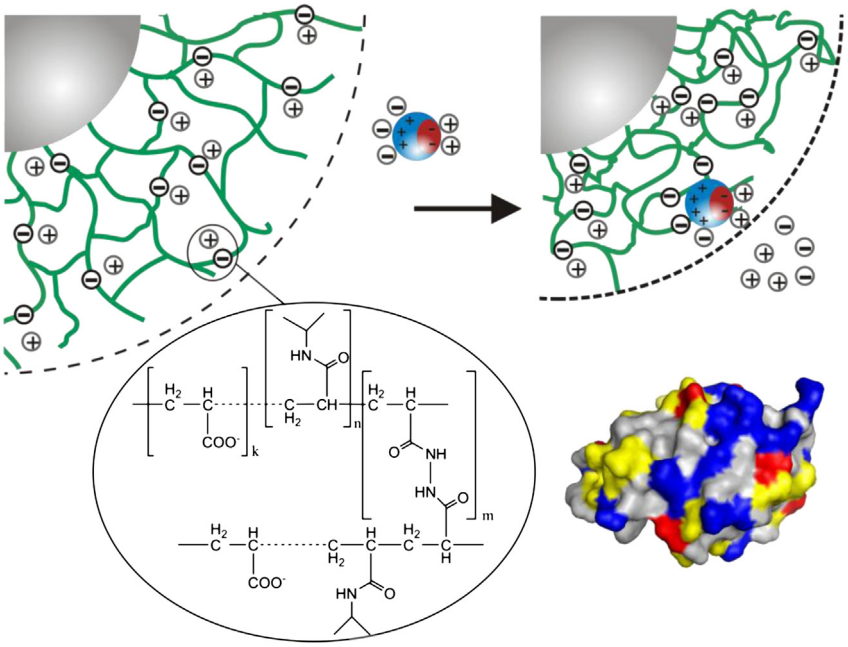

Fig. 8. Top: interaction between a positively charged protein and the negatively charged core–shell microgel. The dashed line illustrates the dimensions of the gel network. The protein is protonated by the electrostatic potential of the polymer network when it enters the gel network. The protein is attracted by the charged network through electrostatic and non-electrostatic interactions which induce microgel deswelling. Bottom left: chemical structure of the crosslinked p(NiPAm-co-AAc) shell. Bottom right: structure of lysozyme (*chicken egg white*, PDB: 193L). The amino acids are colored as according to their polarity and charge: Positive (blue), negative (red), polar (yellow), hydrophobic (gray). Taken from Ref. [42].

segments. The excellent description by the combination of the two forces could be argued from the fact that the hydrophobic term was independent of the concentration of added salt. Thus, a full quantitative modeling of protein uptake by a weakly charged gel could be done in terms of a simple theory using well-defined and intelligible parameters as e.g. the number of hydrophobic contacts per protein molecule. The entire approach is general and can be easily extended to mixtures of proteins.

Fig. 8 summarizes the finding on weakly charged microgels in a schematic fashion. Here another important effect is shown, namely the shrinkage of the microgel layer upon uptake of protein. Obviously, the bound protein carries its own surface charge shown here for the case of lysozyme. This charge neutralizes a part of the opposite charge of the network thus releasing some salt ions into the bulk phase. The shrinking of the microgel layer is of considerable magnitude [43] and must be taken into account in a quantitative treatment of the interaction of proteins with charged gels [44].

For the case of *strongly charged* spherical polyelectrolyte brushes an additional effect must be taken into account as shown schematically in Fig. 9. The overall structure of the SPB is mainly determined by the marked osmotic pressure of the counterions confined within the brush layer. The strongly charged chains of the bound polyelectrolyte become multivalent counterions of the proteins by closely interacting with the surface patches of opposite charge [30–32]. A semi-quantitative model taking into account counterion release [115] was presented recently [31]. In particular,

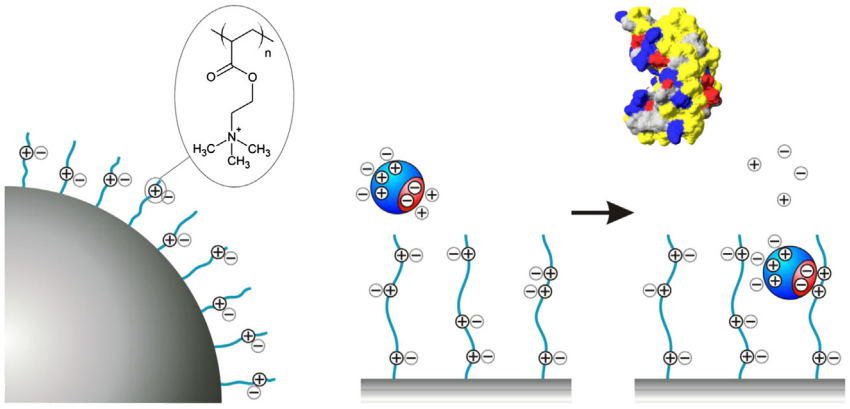

Fig. 9. Protein binding to polyelectrolyte chains attached to a colloidal particle. Left: representation of a positively charged SPB particle and the chemical structure of the cationic polymer in the brush: MAETA. The core-to-shell ratio for the SPB is depicted to scale. Right: electrostatic interaction of a positively charged SPB particle with an overall positively charged protein. The surface of a negatively charged protein consists of patches of positive charge. This positively charged patch (blue) can replace the counterions associated with the negatively charged polymer, causing the release of the counterions associated with both the polymer and the protein. Top right: structure of RNase A (bovine, PDB: 1FS3). The amino acids are colored as follows: positive residues (blue), negative residues (red), polar residues (yellow) and hydrophobic residues (gray). Taken from Ref. [32].

this mechanism is also operative if the brush layer and the protein have the same net charge (adsorption on the "wrong side" of the isoelectric point [28,30,31]). For the adsorption of RNase A to a cationic brush layer, the analysis by ITC demonstrated that the driving force is entirely entropic [32]. For an extensive discussion of counterion release and its relation to protein adsorption on brush layers the reader is deferred to a recent review [47]. While the model is not quantitative yet, the predicted correlation between the Donnan pressure within the brush layer and amount of adsorbed protein was shown for a number of systems [116]. Also, proteins are released in a controlled fashion when ionic strength is raised [82,117]. Finally, the analysis of the composites of proteins and the SPB by SAXS demonstrates that the proteins sit directly on polyelectrolyte chains [80], that is, they slide along the charged chains when entering the brush layer (see below).

Summarizing this part it is fair to state that the interaction of proteins with weakly charged networks is well-understood on a semi-quantitative level. In case of the strongly charged brush layers two additional factors are clearly identified, namely counterion release and charge reversal (see also Refs. [118,119] for further details).

4.2. Secondary and tertiary structure

4.2.1. Analysis by FT-IR

FT-IR spectroscopy can be used to analyze the protein structure after immobilization into a dense microgel network [42]. This is shown in Fig. 10. Here the spectra of a negatively charged pNiPAm microgel are plotted before and after adsorption of lysozyme (Fig. 10a) [42]. Due to the presence of amide bonds in the carrier, the IR spectrum of the particle is dominated by the amide I and II vibrational mode as well. The analysis of these data, however, showed that the secondary structure analysis of the proteins bound to these microgels is not compromised by the absorption of the microgel. Fig. 10b compares the FT-IR spectrum of the free protein with the one of the adsorbed lysozyme, which has been received from the difference spectrum of the protein loaded and pure microgel particle. The information of the protein secondary structure in case of the adsorbed and free lysozyme was obtained by analyzing the FT-IR data using a PLS algorithm.

Using this method the β-sheet and α-helix content of the bound protein was determined to $(2 \pm 3)\%$ and $(30 \pm 4)\%$, respectively. These values are comparable to the values found for free lysozyme determined by us and others [42,102]. Concluding these results, the protein remains intact despite of the strong electrostatic and non-electrostatic interactions between the protein and the polymer chains of the microgel. On the other hand, protonation of the protein as observed during its uptake by the charged microgel [43] is not expected to cause conformational changes of the secondary structure in as much lowering the pH value from pH = 7 to pH = 5 has no effect on the secondary structure of lysozyme in solution [120]. Hence, significant unfolding or denaturation is not observed for proteins immobilized into the microgel networks. These particles may therefore have use in biotechnological applications.

4.2.2. Analysis by fluorescence

Labeling of proteins with fluorescent probes or using of fluorescent proteins allows the use of fluorescence microscopy and fluorescence spectroscopy to visualize the uptake of proteins by particles and to study the structural properties of the adsorbed proteins. In our previous study we used the green fluorescent protein mEosFP as direct probe to monitor its uptake by the 100 nm thick brush layer of single SPB particles using ultrasensitive confocal fluorescence microscopy [82]. At low ionic strength the SPB particles were able to incorporate up to 30 000 protein molecules resulting in highly fluorescent spots in the microscopy image while raising the salt concentration to ~250 mM led to the complete release of mEosFP. The structural integrity of the protein in the adsorbed state can be assessed by analyzing the photophysical properties of mEosFP before, during, and after its interaction with the polyelectrolyte chains of the SPB particle. Fluorescence lifetime measurements are sensitive toward environmental changes and may give further information on the tertiary structure. The analysis of the exponential decay of fluorescence of free mEosFP and adsorbed mEosFP yielded accelerated fluorescence decay in densely loaded SPB particles. The shorter lifetime resulted in a quenching of the fluorescence emission intensity from protein molecules inside the brush by ~50%. In contrast, the fluorescence lifetime of mEosFP molecules after desorption from the SPB particles were comparable to the value of mEosFP before its interaction with the particle indicating that the protein retains its native conformation [82].

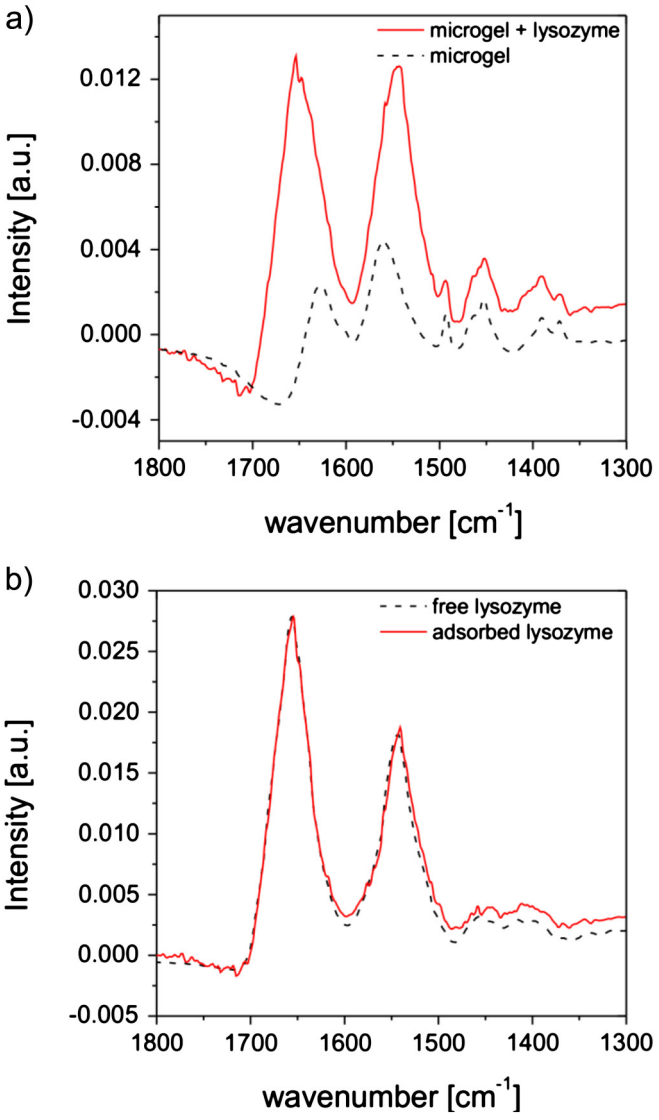

Fig. 10. a) FT-IR spectra of the charged microgel before and after adsorption of lysozyme in 10 mM MOPS pH 7.2 at 298 K. The spectra are scaled a concentration of 1 wt% microgel particles. Particles with immobilized lysozyme carry 660 mg protein per gram microgel. b) FT-IR spectra of free and adsorbed lysozyme. The spectrum of adsorbed spectrum is the difference spectrum of the protein loaded microgel and pure microgel. The protein spectra are normalized to the same lysozyme concentration. Taken from Ref. [42].

4.2.3. Tertiary structure

Measuring the catalytic activity of bound enzymes by suitable assays [121,122] or by ITC [76] provides a direct measure for possible distortions of the tertiary structure. Evidently, this analysis must be done in terms of the classical Michaelis–Menten kinetics

$$v = \frac{k_{cat}[E][S]}{K_m + [S]} \tag{18}$$

where $[S]$ is the substrate concentration, K_m is the Michaelis–Menten constant; $[E]$ is the total protein concentration and k_{cat} is the turnover number. The latter quantity gives a precise measure for any distortion of the active center of the enzyme.

Investigations carried out on enzymes immobilized on SPB particles [76,112,123] demonstrated that the activity may be slightly less than in free solution. Microgels, on the other hand, have turned out to be ideal "nano-reactors": Here it could be shown that proteins may have higher activities than in free solution [41,42]. Fig. 11 demonstrates this finding and the respective analysis using β-D-glucosidase bound to an uncharged microgel [41]. The Lineweaver–Burk plots of the free and incorporated enzyme shown in Fig. 11a were measured at 298 and 317 K, respectively. The lowered slopes of the plots obtained for the immobilized enzymes lead to higher turnover numbers for the β-D-glucosidase molecules located within the microgel network both below and above the LCST of pNiPAm. These observations suggest that the enzyme remains intact after incorporation into the gel network. This is even shown more precisely in the Arrhenius plots obtained for β-D-glucosidase in solution and for enzyme molecules incorporated into the network (Fig. 11b). It is clearly shown that k_{cat} of the enzyme in the bound state is of some magnitudes larger than the values calculated for β-D-glucosidase dissolved free in solution. The increase of the hydrophobicity and the drastic volume change upon temperature increase do not induce changes of the folded state of the protein. The weak retardation of the catalytic activity at temperatures around the LCST indicates an emerging influence of the deswelling microgel network on the free diffusion of the substrate. This effect, however, is very weak and does not prevent the conversion of ortho-nitrophenyl-β-D-glucopyranoside at temperatures above the LCST. Besides the enhanced activity of immobilized β-D-glucosidase we observed altered amide I and II bands in the FT-IR spectrum of the bound protein which suggest the formation of hydrogen bonds between the polymer chains of the microgel and the protein [41]. The latter may account for the increase of the catalytic activity of β-D-glucosidase during its interaction with the microgel network.

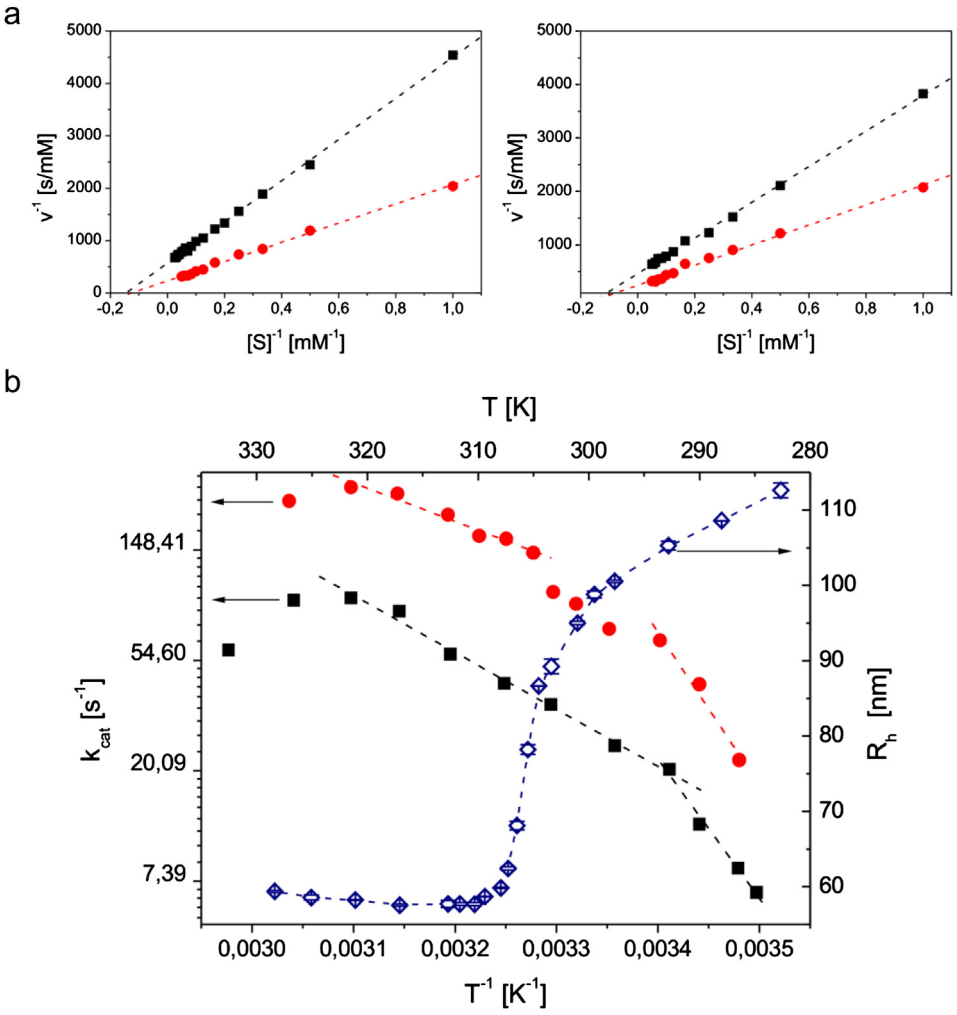

Fig. 11. a) Lineweaver-Burk plots for the hydrolysis of ortho-nitrophenyl-β-D-glucopyranoside catalyzed by immobilized (●) and native β-D-glucosidase (■) at 20 °C (left) and 40 °C (right) in 10 mM MOPS buffer pH 7.2. b) Arrhenius plots obtained for native (■) and immobilized β-D-glucosidase (●). The enzyme concentration was located between 0.005 and 0.01 g L^{-1} (native enzyme) and 0.0035–0.01 g L^{-1} (bound β-D-glucosidase), respectively, and the substrate concentration was varied between 1.0 and 20.0 mM. The dashed lines are linear fits of the experimental data. In addition, the hydrodynamic radius R_h of the carrier is shown as function of temperature T (◇). Taken from Ref. [41].

Microgels carrying a negative net charge were also found to be suitable protein carriers having a beneficial influence on the function of enzymes [43]. The activity test of lysozyme adsorbed to the negatively charged microgel network demonstrated an increased activity of lysozyme in the adsorbed state. The modified activity is closely related to the lowered pH value within the charged network caused by the electrostatic potential of the fixed charges in the gel. In particular, the turnover number of the adsorbed enzyme corresponds to the activity of lysozyme in solution in the protonated state at its pH optimum (pH ~ 5). These investigations suggest that the pronation state and, thus, the activity of adsorbed enzymes may be adjusted by tuning the electrostatic potential of the particles through the amount of fixed charges and the salt concentration [43].

4.2.4. Quaternary structure of adsorbed proteins: SAXS

The analysis of bound proteins by SAXS has demonstrated that the proteins are closed correlated with the chains of the polyelectrolyte layer [78,79,81]. SAXS may also be used to analyze the quaternary structure of bound proteins at least in a semi-quantitative fashion. Fig. 12 shows this for the example of β-lactoglobulin bound to an anionic spherical polyelectrolyte brush [81]. The precise analysis by SAXS conducted in Ref. [81] showed that β-lactoglobulin is slightly aggregated within the brush layer. This is to be expected for the lower pH within the brush layer. The entire analysis demonstrates that SAXS is capable of analyzing the quaternary structure of adsorbed proteins under suitable conditions.

4.3. Kinetic studies of protein adsorption

4.3.1. Analysis by fluorescence spectroscopy

Unlike the kinetic studies of protein adsorption on micron-sized particles [124,125] the uptake of protein by colloidal particles cannot be visualized by microscopic techniques but needs to be studied by other methods, such as fluorescence spectroscopy and SAXS. In our recent work we quantified the adsorption of proteins by negatively charged microgel particles as a function of time by monitoring the fluorescence intensity of fluorescein-labeled lysozyme (lysozyme^{FITC}) with time (Fig. 13) [43]. Upon uptake into the gel network the fluorescence intensity of the labeled protein is drastically reduced. The loss of fluorescence of the fluorescent probe is directly correlated with the adsorption of lysozyme and is caused by the lowered pH value within the charged microgel network. Fig. 14 depicts the uptake of lysozyme into the charged gel layer as function of time for different protein concentrations at low salt concentration. These experiments demonstrate that lysozyme^{FITC} appears to adsorb in two steps which drastically differ in their time regimes. This is indicated by the first sharp decrease of the intensity within the first seconds after microgel injection (fast regime) which is followed by a much slower step (slow regime). The latter continues over several hundred seconds in contrast to the first step. Apparently the fast regime of protein binding seems to be controlled by the diffusion of the protein toward the network and its uptake by the shell. This process can be quantified using the kinetic Langmuir model (eq. (12)).

The fast motion of the proteins into the microgel needs to be split up into two contributions which is explained by the differing transport properties in the bulk and gel phase: i) The diffusion of the proteins in the bulk solution to the microgel surface which is quantified by k_D; ii) and the protein uptake by the gel network which is characterized by k_i (see Fig. 7). Applying the theoretical model outlined in Section 3.3 to the kinetic data acquired for lysozyme binding gives access to the time constants k_D and k_i. In this case k_D and k_i were determined to be of comparable size.

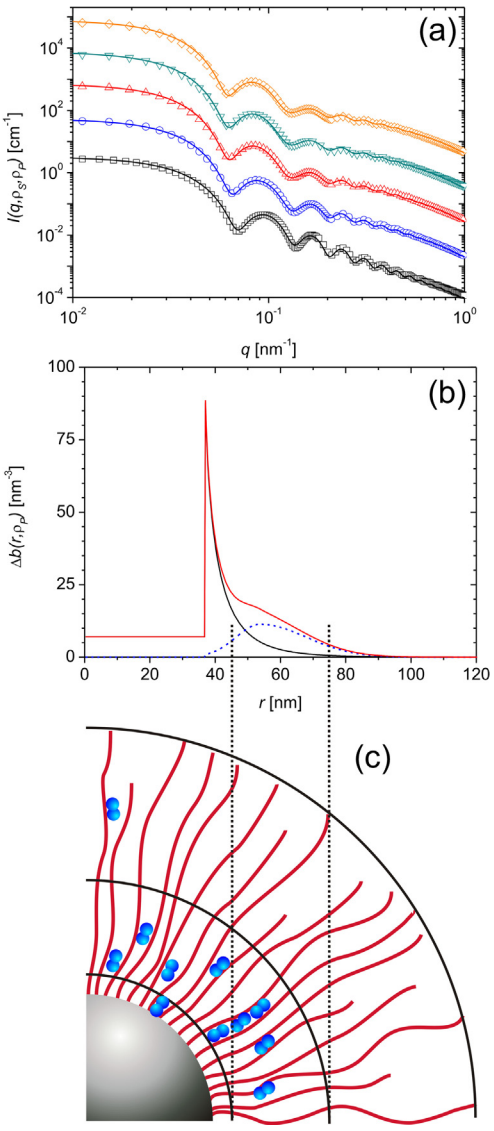

Fig. 12. Experimentally determined scattering intensity $I(q)$ of spherical polyelectrolyte brush particles. Parameter is the different amounts of added β-lactoglobulin (symbols). The particle number density is $\rho_s = 2.01 \times 10^{-8}$ nm^{-3}, while the protein number density increases from bottom to top according to $\rho_p/\rho_s = 1629$ (101 mg BLG/g SPB), 6514 (400 mg BLG/g SPB), 9771 (600 mg BLG/g SPB), 12,214 (750 mg BLG/g SPB), 16,286 (990 mg BLG/g SPB). The upper four data sets have been shifted by a constant factor. The solid lines depict the calculated scattering intensities. In panel (b) the electron density profiles of the pure brush ($\Delta b(r, \rho_p = 0)$, black line), the brush with adsorbed proteins ($\Delta b(r, \rho_p)$, red line) and the pure adsorbed proteins ($\Delta b_p(r, \rho_p)$, blue dashed line) are shown in for a core radius of 37 nm (c): Cutout of a 2-dimensional representation of the SPB with the distribution of 400 mg BLG/g SPB derived from (b). The protein molecules which are in the outer part of the brush layer can be released by extensive ultrafiltration. The presented illustration is up to scale. Taken from Ref. [81].

The kinetic analysis was complemented with the thermodynamic binding study performed by ITC which gives access to the binding constant K. From the known values of K and k_{on} one can calculate the desorption rate constant k_{off}. The latter was determined to ~0.5 s^{-1} which translates into a mean residence time of lysozyme^{FITC} on the microgel network k_{off}^{-1} of around 2 s. However, Fig. 14 suggests a two-step binding mechanism where only 90% of the protein is taken up in the fast binding regime. The remaining protein fraction is adsorbed much more slowly in a following step. This slow binding regime is described by a time constant of a few hundred seconds and may be caused by collective phenomena:

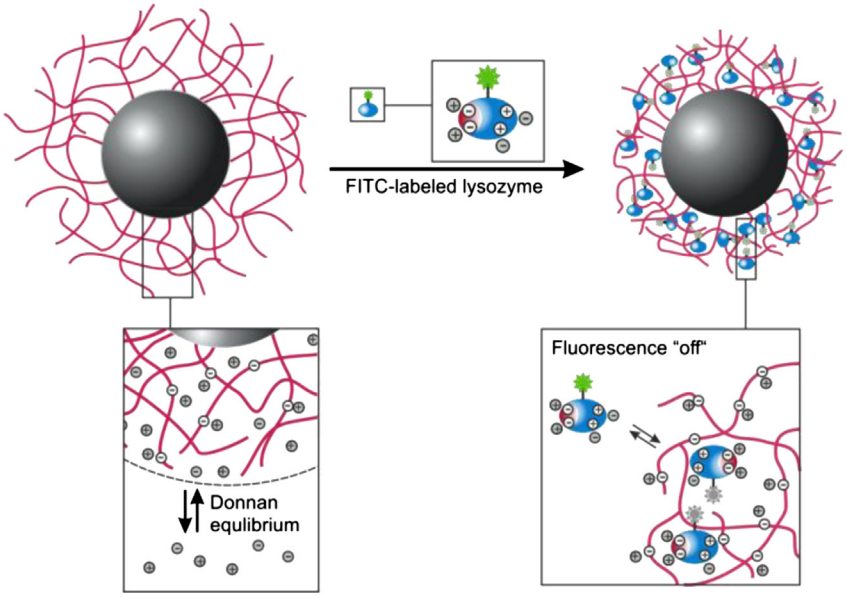

Fig. 13. Interaction between fluorescein-labeled lysozyme and a core–shell microgel. The core of the particle consists of polystyrene and the shell contains a network of poly-(N-isopropylacrylamide) (pNiPAm) and acrylic acid. The concentration of the ions inside is determined by the ion concentration of the outer solution through the Donnan-equilibrium. The lower pH within the network and mutual quenching of the fluorophores leads the decrease of the fluorescence intensity that can be analyzed as the function of time. These data are used for the quantitative analysis of the kinetics of protein uptake.

Since the binding of oppositely charged proteins causes shrinking of the microgel network, the decrease of the microgel volume with time may lead to the rearrangement of bound proteins within the microgel. The deswelling of the microgel and the reorientation of the protein molecules toward the charged polymer certainly continues over longer time scales resulting in protein uptake over several hundred seconds (slow binding regime).

4.3.2. Analysis by SAXS

SAXS can be used in special cases to monitor the kinetics of the uptake of proteins into SPB [80]. Fig. 15 shows the main result from the latter analysis in a schematic fashion [80]: The protein molecules are sliding along the polyelectrolyte chains. This result has been concluded from the fact that the total amount of adsorbed protein τ_{ads} determined from the analysis of the SAXS-data increases as $t^{0.25}$ and not as $t^{0.5}$ as expected for a purely diffusive transport. The electrostatic interaction increases when the proteins are moving from outside into the brush layer along the radial direction and the proteins are driven into the brush by the inhomogeneous electric field. A simple model based on this fact leads to the exponent 0.25 as observed experimentally [78]. From the estimated time constant of this process it is clear that this motion must be a sliding along the chains of the polyelectrolyte, not a movement of

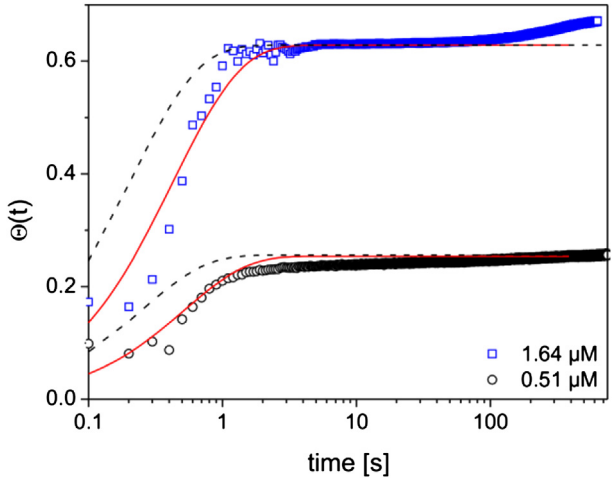

Fig. 14. Uptake of lysozyme by the microgel as function of time: Fraction of occupied binding sites Θ as function of time after addition of 0.029 g L^{-1} microgel dispersion in to a solution of lysozyme^{FITC} of two different concentrations. The time of microgel injection was set to $t = 0$. The experiments were done in 10 mM MOPS buffer pH 7.2 at 293 K. The solid lines represent the fit according to eq. (12) the dashed lines represent the theoretical curve predicted by eq. (12) with k_{on} set to k_D/N, *i.e.*, $k_i = \infty$ in eq. (14). Taken from Ref. [43].

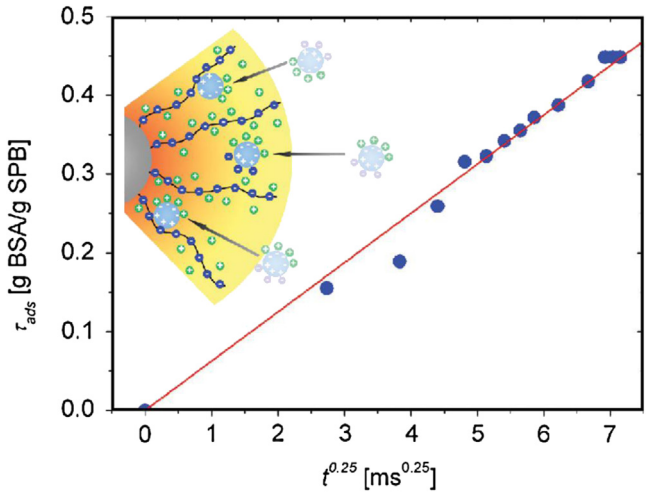

Fig. 15. Overall amount of adsorbed protein, τ_{ads} as a function of time. τ_{ads} has been obtained from the evaluation of the electron density profiles measured by SAXS. The inset schematically depicts the motion of proteins through the polyelectrolyte layer driven by the inhomogeneous electric field within the brush layer. Taken from Ref. [80].

the proteins in aqueous solution. The latter process would be much faster and not anymore by measurable by the time-resolved SAXS-technique used in Ref. [80].

5. Conclusions

The foregoing discussion has demonstrated that we now have a well-developed set of tools that allow us to study the binding of proteins to functional nanoparticles in a detailed fashion. ITC and SAXS lead to a precise determination of the adsorption isotherm whereas spectroscopic techniques as FT-IR give information about the secondary structure of the adsorbed proteins. The dynamics of adsorption can now be determined precisely by fluorescence spectroscopy and by SAXS. Information about the distribution of the bound proteins is available through SAXS. Last not least, activity measurements of bound enzymes lead to a precise assessment of the tertiary structure and qualitative information about possible aggregation of bound proteins may become available through SAXS as well. All data furnish the firm basis for a theoretical modeling of protein adsorption to functional polymeric layers. Work along these lines is under way.

Acknowledgment

The authors acknowledge financial support by the Helmholtz Virtual Institute, and by the Deutsche Forschungsgemeinschaft, SPP “Intelligente Hydrogele”, and the “International Research Training Group 1524”.

References

[1] Nel AE, Madler L, Velegol D, Xia T, Hoek EMV, Somasundaran P, et al. Nat Mater 2009;8:543–57.
[2] Moyano DF, Rotello VM. Langmuir 2011;27:10376.
[3] Cukalevski R, Lundqvist M, Oslakovic C, Dahlback B, Linse S, Cedervall T. Langmuir 2011;27:14360–9.
[4] Dobrovolskaia MA, Germolec DR, Weaver JL. Nat Nanotechnol 2009;4:411–4.
[5] Xu X, Lenhoff AM. J Phys Chem B 2008;112:1028–40.
[6] Rana S, Yeh YC, Rotello VM. Curr Opin Chem Biol 2010;14:828–34.
[7] Lynch I, Salvati A, Dawson KA. Nat Nanotechnol 2009;4:546–7.
[8] Klein J. Proc Natl Acad Sci USA 2007;104:2029–30.
[9] Walczyk D, Bombelli FB, Monopoli MP, Lynch I, Dawson KA. J Am Chem Soc 2010;132:5761–8.
[10] Monopoli MP, Walczyk D, Campbell A, Elia G, Lynch I, Bombelli FB, et al. J Am Chem Soc 2011;133:2525–34.
[11] Caracciolo G, Pozzi D, Capriotti AL, Cavaliere C, Foglia P, Amenitsch H, et al. Langmuir 2011;27:15048–53.
[12] Casals E, Pfaller T, Duschl A, Oostingh GJ, Puntes V. ACS Nano 2010;4:3623–32.
[13] Lundqvist M, Stigler J, Cedervall T, Berggård T, Flanagan MB, Lynch I, et al. ACS Nano 2011;5:7503–9.
[14] Khandare J, Calderon M, Dagia N, Haag R. Chem Soc Rev 2012;41:2824–48.
[15] Ganesan R, Kratz K, Lendlein A. J Mater Chem 2010;20:7322–31.
[16] Scharnagl N, Lee S, Hiebl B, Sisson A, Lendlein A. J Mater Chem 2010;20:8789–802.
[17] Dash PR, Read ML, Barrett LB, Wolfert M, Seymour LW. Gene Ther 1999;6:643–50.
[18] Owens DE, Peppas NA. Int J Pharm 2006;307:93–102.
[19] Vroman L, Adams AL. Surf Sci 1969;16:438–46.
[20] Jung SY, Lim SM, Albertorio F, Kim G, Gurau MC, Yang RD, et al. J Am Chem Soc 2003;125:12782–6.
[21] Noh H, Vogler EA. Biomaterials 2007;28:405–22.
[22] Fang F, Szleifer I. Biophys J 2001;80:2568–89.
[23] Xia XR, Monteiro-Riviere NA, Riviere JE. Nat Nanotechnol 2010;5:671–5.
[24] Treuel L, Nienhaus GU. Biophys Rev 2012;4:137–47.
[25] Weber M, Bujotzek A, Andrae K, Weinhart M, Haag R. Mol Simulation 2011;37:899–906.
[26] Herrwerth S, Eck W, Reinhardt S, Grunze M. J Am Chem Soc 2003;125:9359–66.
[27] Heyes CD, Groll J, Möller M, Nienhaus GU. Mol Biosyst 2007;3:419–30.
[28] Borisov OV, Ballauff M. Curr Opin Colloid Interf Sci 2006;11:316–23.
[29] Ballauff M. Progr Polym Sci 2007;32:1135–51.
[30] Wittemann A, Haupt B, Ballauff M. Phys Chem Chem Phys 2003;5:1671.
[31] Henzler K, Haupt B, Lauterbach K, Wittemann A, Borisov O, Ballauff M. J Am Chem Soc 2010;132:3159–63.
[32] Becker AL, Welsch N, Schneider Ch, Ballauff M. Biomacromolecules 2011;12:3936.
[33] Hollmann O, Czeslik C. Langmuir 2006;22:3300.
[34] Evers F, Reichhart Ch, Steitz R, Tolan M, Czeslik C. Phys Chem Chem Phys 2010;12:4375–82.
[35] Uhlmann P, Houbenouv N, Brenner N, Grundke K, Burkert S, Stamm M. Langmuir 2007;23:57–64.
[36] Uhlmann P, Merlitz H, Sommer J-U, Stamm M. Macromol Rapid Comm 2009;30:732–40.
[37] Lu Y, Ballauff M. Polymer 2007;48:1815–23.
[38] Lu Y, Ballauff M. Progr Polym Sci 2011;36:767–92.
[39] Lindman S, Lynch I, Thulin E, Nilsson H, Dawson KA, Linse S. Nano Lett 2007;7:914–20.
[40] Cohen Stuart MAC, Huck WTS, Genzer J, Muller M, Ober C, Stamm M, et al. Nat Mater 2010;9:101–13.
[41] Welsch N, Wittemann A, Ballauff M. J Phys Chem B 2009;113:16039–45.
[42] Welsch N, Becker AL, Dzubiella J, Ballauff M. Soft Matter 2012;8:1428–36.
[43] Welsch N, Dzubiella J, Graebert A, Ballauff M. Soft Matter 2012;8:12043–52.
[44] Yigit C, Welsch N, Ballauff M, Dzubiella J. Langmuir 2012;28:14373–85.
[45] Rashin AA, Honig B. J Mol Biol 1984;173:515–21.
[46] Fenley MO, Russo C, Manning GS. J Phys Chem B 2011;115:9864.
[47] Becker AL, Henzler K, Welsch N, Ballauff M, Borisov O. Curr Opin Colloid Interf Sci 2012;17:90–6.
[48] Wittemann A, Lu Y, Ballauff M. Macromol Rapid Comm 2009;30:806–15.
[49] Behrens SH, Borkovec M, Schurtenberger P. Langmuir 1998;14:1951–4.
[50] Schneider Ch, Jusufi A, Farina R, Pincus P, Tirrell M, Ballauff M. Phys Rev E 2010;82:011401.
[51] Crassous JJ, Siebenbürger M, Ballauff M, Drechsler M, Henrich O, Fuchs MJ. Chem Phys 2006;125:204906.
[52] Crassous JJ, Wittemann A, Siebenbürger M, Schrinner M, Drechsler M, Ballauff M. Colloid Polym Sci 2008;286:805–12.
[53] Crassous JJ, Rochette CN, Wittemann A, Schrinner M, Ballauff M, Drechsler M. Langmuir 2009;25:7862–71.
[54] Hoffmann M, Jusufi A, Schneider Ch, Ballauff M. J Colloid Interface Sci 2009;338:566–72.
[55] Jimenez ML, Delgado AV, Ahualli S, Hoffmann M, Witteman A, Ballauff M. Soft Matter 2011;7:3758–62.
[56] Borisov OV, Birshtein TM, Zhulina EB. J Phys (France) 1994;4:913–29.
[57] Pincus P. Macromolecules 1991;24:2912–9.
[58] Sierra-Martin B, Lietor-Santos JJ, Fernandez-Barbero A, Nguyen TT, Fernandez-Nieves A. Swelling thermodynamics of microgel particles. In: Fernandez-Nieves A, Wyss HM, Mattsson J, Weitz DA, editors. Microgel suspensions: fundamentals and applications. Weinheim, Germany: Wiley-VCH; 2011.
[59] Biesheuvel PM, Wittemann A. J Phys Chem B 2005;109:4209–14.
[60] de Vos WM, Biesheuvel PM, de Keizer A, Klein JM, Cohen Stuart MA. Langmuir 2008;24:6575–84.
[61] Chaudhari A, Thota J, Kumar CV. Microporous Mesoporous Mater 2004;75:281–91.
[62] Cedervall T, Lynch I, Lindman S, Berggard T, Thulin E, Nilsson H, et al. Proc Natl Acad Sci USA 2007;104:2050–5.
[63] De M, You CC, Srivastava S, Rotello VM. J Am Chem Soc 2007;129:10747–53.
[64] You CC, Agasti SS, Rotello VM. Chem Eur J 2008;14:143–50.
[65] Duff MR, Kumar CV. Langmuir 2009;25:12635–43.
[66] Duff MR, Kumar CV. J Phys Chem B 2009;113:15083–9.
[67] Zhu RR, Wang WR, Sun XY, Liu H, Wang SL. Toxicol Vitro 2010;24:1639–47.
[68] Martinez-Barbosa ME, Cammas-Marion S, Bouteiller L, Vauthier C, Ponchel G. Bioconjug Chem 2009;20:1490–6.
[69] Baier G, Costa C, Zeller A, Baumann D, Sayer C, Araujo PHH, et al. Macromol Biosci 2011;11:628–38.
[70] Rieger J, Freichels H, Imberty A, Putaux JL, Delair T, Jerome C, et al. Biomacromolecules 2009;10:651–7.
[71] Chen KM, Xu YS, Rana S, Miranda OR, Dubin PL, Rotello VM, et al. Biomacromolecules 2011;12:2552–61.
[72] Chaires JB. Biophys Chem 1997;64:15–23.
[73] Winzor DJ, Jackson CM. J Mol Recognit 2006;19:389–407.
[74] Horn JR, Russell D, Lewis EA, Murphy KP. Biochemistry 2001;40:1774–8.
[75] Horn JR, Brandts JF, Murphy KP. Biochemistry 2002;41:7501–7.
[76] Henzler K, Haupt B, Ballauff M. Anal Biochem 2008;378:184–9.
[77] Dingenouts N, Bolze J, Pötschke D, Ballauff M. Adv Polym Sci 1999;144:1.
[78] Rosenfeldt S, Wittemann A, Ballauff M, Breininger E, Bolze J, Dingenouts N. Phys Rev E 2004;70:061403.
[79] Henzler K, Wittemann A, Breininger E, Ballauff M, Rosenfeldt S. Biomacromolecules 2007;8:3674.
[80] Henzler K, Rosenfeldt S, Wittemann A, Harnau L, Finet S, Narayanan Th, et al. Phys Rev Lett 2009;100:158301–4.
[81] Henzler K, Haupt B, Rosenfeldt S, Harnau L, Narayanan Th, Ballauff M. Phys Chem Chem Phys 2011;13:17599.
[82] Anikin K, Röcker C, Wittemann A, Wiedenmann J, Ballauff M, Nienhaus GU. J Phys Chem B 2005;109:5418.
[83] Czeslik C, Jansen R, Ballauff M, Wittemann A, Royer CA, Gratton E, et al. Phys Rev E 2004;69:021401.
[84] Czeslik C, Jackler G, Hazlett T, Gratton E, Steitz R, Wittemann A, et al. Phys Chem Chem Phys 2004;6:5557–63.

[85] Lacerda SHDP, Park JJ, Meuse C, Pristinski D, Becker ML, Karim A, et al. ACS Nano 2010;4:365–79.
[86] Röcker C, Pötzl M, Zhang F, Parak WJ, Nienhaus GU. Nat Mater 2009;4:577–80.
[87] Bunz UHF, Rotello VM. Angew Chem Int Ed 2010;49:3268–79.
[88] De M, Rana S, Akpinar H, Miranda OR, Arzivo RR, Bunz UHF, et al. Nat Chem 2009;1:461–5.
[89] Vanstokkum IHM, Linsdell H, Hadden JM, Haris PI, Chapman D, Bloemendal M. Biochemistry 1995;34:10508–18.
[90] Barrera FN, Garzón MT, Gómez J, Neira JL. Biochemistry 2002;41:5743–53.
[91] Wittemann A, Ballauff M. Anal Chem 2004;76:2813.
[92] Wittemann A, Ballauff M. Macromol Biosci 2005;5:13–20.
[93] Servagent-Noinville S, Revault M, Quiquampoix H, Baron M-H. J Colloid Interface Sci 2000;221:273–83.
[94] Xiao Q, Huang S, Qi Z-D, Zhou B, He Z-K, Liu Y. Biochim Biophys Acta Proteins Proteomics 2008;1784:1020–7.
[95] Karajanagi SS, Vertegel AA, Kane RS, Dordick JS. Langmuir 2004;20:11594–9.
[96] Jiang X, Jiang J, Jin Y, Wang E, Dong S. Biomacromolecules 2005;6:46–53.
[97] Mandal H, Kraatz H-B. J Am Chem Soc 2007;129:6356–7.
[98] Sun S, Hu J, Tang H, Wu P. J Phys Chem B 2010;114:9761–70.
[99] Pühse M, Keerl M, Scherzinger C, Richtering W, Winter R. Polymer 2010;51:3653–9.
[100] Keerl M, Smirnovas V, Winter R, Richtering W. Angew Chem Int Ed 2008;47:338–41.
[101] Surewicz WK, Mantsch HH, Chapman D. Biochemistry 1993;32:389–94.
[102] Dousseau F, Pezolet M. Biochemistry 1990;29:8771–9.
[103] Haaland DM, Thomas EV. Anal Chem 1988;60:1193–202.
[104] Jackler G, Wittemann A, Ballauff M, Czeslik C. Spectroscopy 2004;18:289–99.
[105] Felsovalyi F, Mangiagalli P, Bureau C, Kumar SK, Banta S. Langmuir 2011;27:11873–82.
[106] Bharti B, Meissner J, Findenegg GH. Langmuir 2011;27:9823–33.
[107] Louguet S, Kumar AC, Guidolin N, Sigaud G, Duguet E, Lecommandoux S, et al. Langmuir 2011;27:12891–901.
[108] Cullen SP, Liu X, Mandel IC, Himpsel FJ, Gopalan P. Langmuir 2008;24:913–20.
[109] Hoshino Y, Koide H, Furuya K, Haberaecker WW, Lee SH, Kodama T, et al. Proc Natl Acad Sci USA 2012;109:33–8.
[110] Dill KA, Bromberg S. Molecular driving forces. New York: Taylor & Francis Group; 2003.
[111] Cernik M, Borkovec M, Westall JC. Langmuir 1996;12:6127–37.
[112] Haupt B, Neumann Th, Wittemann A, Ballauff M. Biomacromolecules 2005;6:948.
[113] Azizian S. J Colloid Interface Sci 2004;276:47–52.
[114] Jackson MB. Molecular and cellular biophysics. New York: Cambridge University Press; 2006.
[115] Record MT, Anderson CF, Lohman TM. Q Rev Biophys 1978;11:103.
[116] Wittemann A, Ballauff M. Phys Chem Chem Phys 2006;8:5269–75.
[117] Wittemann A, Haupt B, Ballauff M. Z Phys Chem NF 2007;221:113–26.
[118] Leermakers FAM, Ballauff M, Borisov OV. Langmuir 2007;23:3937–46.
[119] De Vos W, Leermakers FAM, de Keizer A, Cohen Stuart MA, Klein JM. Langmuir 2010;26:249–59.
[120] Vertegel AA, Siegel RW, Dordick JS. Langmuir 2004;20:6800–7.
[121] Ghosh P, Yang X, Arvizo R, Zhu ZJ, Agasti SS, Mo Z, et al. J Am Chem Soc 2010;132:2642–5.
[122] Shang W, Nuffer JH, Muñiz-Papandrea VA, Colón W, Siegel RW, Dordick JS. Small 2009;5:470–6.
[123] Neumann T, Haupt B, Ballauff M. Macromol Biosci 2004;4:13.
[124] Li YA, Zhang Z, van Leeuwen HP, Stuart MAC, Norde W, Kleijn JM. Soft Matter 2011;7:10377–85.
[125] Johansson C, Hansson P, Malmsten M. J Phys Chem B 2009;113:6183–93.

Nicole Welsch studied chemistry at the University of Bayreuth, where she received her diploma in 2008 in the group of Professor Dr. M. Ballauff. In 2012 she completed her PhD on the investigation of the interactions of proteins on soft polymeric surfaces including microgels at the Institute of Soft Matter and Functional Materials, Helmholtz-Zentrum Berlin, and at the Humboldt University of Berlin under supervision of Professor Dr. M. Ballauff. Her research interest focuses on polymer colloids and nano-engineered materials for use in biological applications and the characterization of this material in biological media.

Yan Lu received her PhD in 2005 under the supervision of Prof.Dr. H.-J.P.Adler in macromolecular chemistry at Dresden University of Technology. After that, she worked first as post-doctor then research scientist in Prof.Dr. M. Ballauff's group in the University of Bayreuth. Since 2009, she joined the Helmholtz-Zentrum Berlin fürMaterialien und Energie as a group leader in Colloid Chemistry. She was awarded "APi-Prize" in 2005 and "Dr. Hermann-Schnell-Stipendium" in 2011 by the German Chemical Society. Her research interests cover synthesis and characterization of functional hybrid colloidal particles and their application as catalyst, optics and solar-cells.

Joachim Dzubiella received his doctorate in 2002 under the supervision of Prof. C. N. Likos and Prof. H. Löwen in theoretical colloidal physics at the Heinrich-Heine University in Düsseldorf, Germany. After postdoctoral stays with Prof. J.-P. Hansen in Cambridge, UK, and Prof. A. J. McCammon in San Diego, USA, he returned to Germany in 2006 to head an Emmy-Noether research group at the Technical University Munich. Since 2010 he is the group leader for Soft Matter Theory at the Helmholtz-Center Berlin and Professor for Theoretical Physics at the Humboldt-University of Berlin.

Matthias Ballauff studied chemistry at the University of Mainz and got is PhD there in the Institute of Physical Chemistry in 1981. He was a postdoc in the group of P.J. Flory in Stanford from 1981- 1983 and subsequently research associate at the Max-Planck-Institute for Polymer Research in Mainz. From 1990 -2003 he was a professor of polymer science at the University of Karlsruhe. From 2003 to 2009 he hold the chair of Physical Chemistry I at the University of Bayreuth. From 2009 on he is a professor of Experimental Physics at the Humboldt University Berlin and Head of the Institute of Soft Matter and Functional Materials at the Helmholtz-Zentrum Berlin. His interests comprise scattering methods and polymer colloids for applications in materials science and catalysis.